J. Condensed Matter Nucl. Sci. 29 (2019) 177–190

Research Article

Aqueous and Nanostructured CF/LANR Systems Each has Two Electrically Driven Modes

Mitchell R. Swartz*

JET Energy Inc., Wellesley Hills, MA 02481, USA

Abstract

An important difficulty to overcome for success in this field is the recognition and control of the two different electrically driven modes for both aqueous and nanostructured CF/LANR systems. Only one state is the active, desired, excess heat (XSH)-producing state ("mode"). This is demonstrated by presenting calorimetry and other measurements of both modes during a single run, and by confirmation using CMORE spectroscopy. It is fortunate that LANR systems, when active, have distinct calorimetric and CMORE anti-Stokes-XSH linked signatures, because it explains why some CF/LANR systems fail to create "excess heat" (XSH), and reveals unwanted reactions, XSH-quenching reactions and pathways.
 ISSN 2227-3123

Keywords: Biphasic response, CMORE spectroscopy, Excess heat mode, Quenching, Two modes, Two states

1. Introduction

Lattice assisted nuclear reactions (LANR) use hydrogen-loaded alloys to create heat and other products by enabling deuterium fusion under difficult-to-achieve conditions [1]. LANR success is "rewarded" by excess heat (XSH), meaning successful generated *de novo* helium within the lattice ($\sim 10^{12}$ for every watt-second) [2]. However, there are also unwanted reactions and quenching path ways in parallel with the desired reactions of the original method which Fleischmann and Pons taught in March 1989 (aqueous, low impedance Pd/D_2O/Pt). LANR, then called "cold fusion", thus had low efficiency and poor reproducibility which created havoc for the inexperienced in metallurgy, electrochemistry, contamination avoidance, and optimal operating point (OOP) operation [3–6].

This paper reports an important difficulty to overcome for success in this field: the existence of (at least) two electrically driven modes for both aqueous and nanostructured CF/LANR systems. Two-pole calorimetry, gas measurement (O_2, H_2, pH_2O/pD_2O, barometric pressure) and Coherent Multiwavelength Optical Reflection Electric-driven (CMORE) spectroscopy have each separately revealed these two distinct states ("modes") of electrical-driven performance. Importantly, only one state is the active, desired, state, and that is the XSH-producing mode. The two states for an aqueous system during a single run are shown in Fig. 1. One mode is active and heat-producing, the other is not.

*Dr. Mitchell R. Swartz ScD, MD, EE, E-mail: moac@nanortech.com.

 ISSN 2227-3123

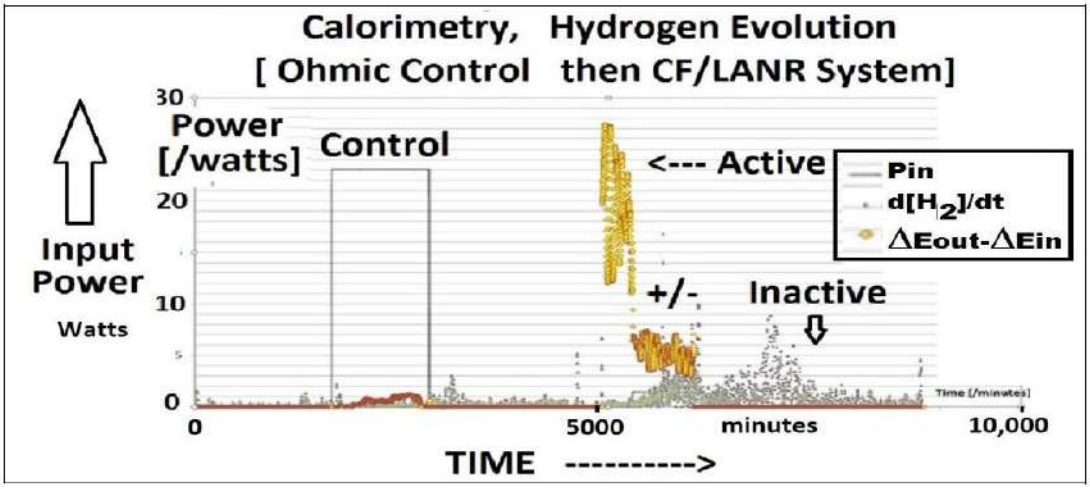

Figure 1. Two electric-drive modes revealed for aqueous NR systems by calorimetry.This figure shows the calorimetry (including incremental power gain, and the rate of XSH- and H_2-production). This aqueous Ni ordinary water system (Pt anode, PHUSOR®-type) shows the two modes in a single run. There is first a control pulse and then three levels of much lower input to the component, showing first much excess power, then an intermediate region, and then mainly hydrogen gas evolution.

2. Background

2.1. Two driven states exist in nature

Two state driven systems, with vastly different performance from each other, already exist in nature. In aviation, there are two states well known, being aerodynamic flight and stalling. A stall does not mean the engines do not work, nor does it mean that the aircraft is not moving. The implications from the performance difference are fierce. The first parallel requires one to note the similarity of shape of the OOP [7–11] (as demonstrated at ICCF-10 by papers [5,6] and open demonstrations [11]) to what is also confirmed as the shape seen for conventional aerodynamics with an airfoil (cf. Fig. 2). The second parallel might follow the fact that ONLY when vectored thrust was used to surpass the stall limit, did there finally evolve a plethora of post-stall avionic technologies. Therefore, we much pay close attention to these different modes.

2.2. Future proves past

Looking backwards, these recent discoveries have confirmed the earlier theories. The possible existence of two states was first heralded by the quasi-1-dimensional model of isotope loading [12,13,7], which thereafter yielded many contributions (codeposition [14], OOP control [7–11], HAD control [15], etc. as shown at ICCF-7 [9], ICCF-10 [5,6], and ICCF-14 [3,4]). Later, the existence of two states was clearly demonstrated for NANOR-type components when electrically driven into avalanche mode at ICCF-19 [16].

Finally, these two electrically driven states were then confirmed by dual beam coherent Raman spectroscopy of electrically driven CF/LANR components (CMORE spectroscopy), including at ICCF-20 [17,18] and ICCF-21 [19], as discussed below.

This paper augments those results with confirmation of two states and demonstrates further uniformity among both aqueous and nanostructured CF/LANR materials, and also presents aqueous experiments using the MOAC, including

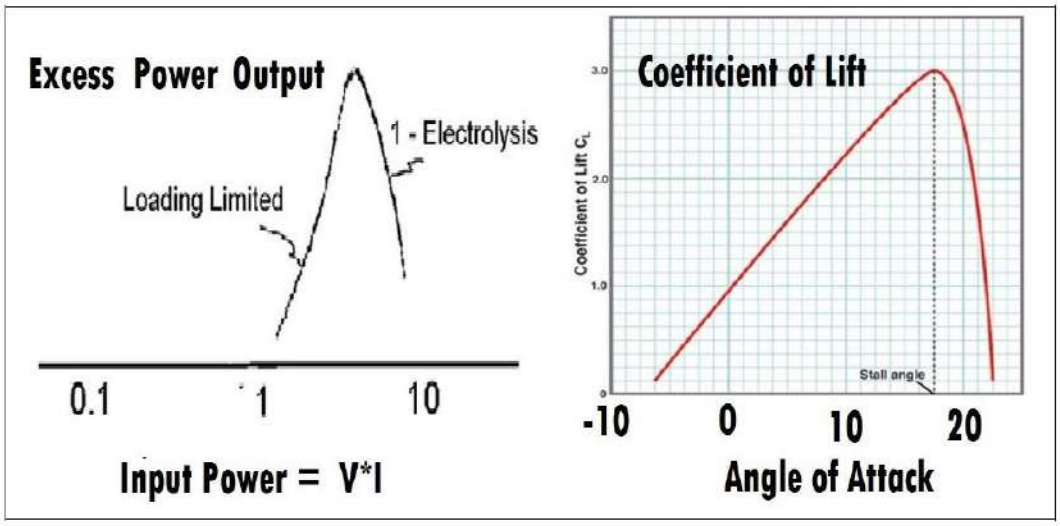

Figure 2. Similar curves describe the two states of driven systems. On the left-hand side is the OOP of aqueous Pd/heavy water vs. platinum anode, and the on the right-hand side is the lift of an aerofoil as a function of attack angle. Notice the peak performance is limited, and further input is clearly not rewarded.

both modes observed during a single run, and confirmation by CMORE spectroscopy. It is confirmed that one mode is active and heat-producing, the other is not.

2.3. CMORE scattering reveals two states

Classic Raman spectroscopy involves the inelastic scattering of light which generates new frequencies which result from the interaction of light the irradiated matter [20]. Raman anti-Stokes scattering results when the irradiated material already contains excited states, and the reflected photons are blue-shifted by the difference in energy between the excited states returning to their ground state. The major problem of the Raman effect is that it produces very weak signals because the photon conversion efficiencies are less than 10^{-18}. However, that is not the case when irradiation is made using coherent lasers which yield a much larger signal because with coherent illumination there results phase-matching conditions and quadratic dependence on the number of local oscillators. Thus, even with the same selection rules, the coherent irradiation Raman effect yields a much greater signal intensity (circa 10^6 times greater) [17–19], and it has yielded a new imaging modality for excited energy states which only appear in working active CF/LANR systems [1,3–11].

Simply put, it offers investigators of condensed matter nuclear science a new diagnostic – in addition to calorimetry and detection of classical emissions. One can easily see the distinguishing optical output in the desired correctly driven active "state" as revealed by the new diagnostic technology. Successful cold fusion systems indicate their activity by a large increase in the aS/S ratio for BOTH active aqueous and nanomaterial CF/LANR systems. There is an XSH-related anti-Stokes peak which is singular and at higher energy. This distinguishing, higher energy anti-Stokes peak (which also heralds phonon gain] is not seen in the "off" state.

As a corollary, from a materials point of view, it appears that acoustic phonons result from, or are required for, an active cold fusion process producing energy gain in its "XSH" mode in both this aqueous system and nanomaterial CF/LANR systems.

3. Experimental

3.1. Aqueous

The aqueous CF/LANR system used for this report is a Ni/H_2O/Pt system which was designed to have a very large electrode area [19,21]. The cathode weighs 4.7 pounds, made from #46 hard drawn smooth nickel wire (0.00399 cm diameter, with an area of circa 240,000 cm^2). The anode was five folded platinized sheets of titanium with an area of $\sim$3200 cm^2, for a surface area ratio of cathode to anode of 75:1. The electrolyte was a dilute carbonate solution (K_2CO_3); circa 0.1 M in distilled water of natural deuteron abundance. Two internal ohmic controls were used. This LANR cell has a 3 l capacity. The methodology of electrically driving this system was discussed at ICCF-10,14 [3–7]. It was electrically driven by a steady direct current electrical drive (2.9 V, 0.50 A; with a measured energy gain of $\sim$4.0 using *V*I* as the electrical input) while it was irradiated by the two lasers while physically maintained in position. Using several ohmic (thermal) and other controls, the anti-Stokes to Stokes (aS/S) ratio was determined when the materials were examined in both the "off" condition including where the desired cold fusion reactions occur.

3.2. Nanomaterial

The NANOR®-type component is the two terminal component with a cylindrical shaped active CF/LANR core. The dry, preloaded NANOR®-type technology makes LANR reactions more accessible. These self-contained, two-terminal nanocomposite ZrO_2–PdNiD CF/LANR components have at their core ZrO_2–PdD nanostructured material. The NANOR® components are smaller than 2 cm length, and with 30–200 mg of active LANR material.

Their "core" contains active ZrO_2–PdD nanostructured material, loaded with additional D to loadings (ratio of D to Pd) of more than 130%, but shallow traps are not ruled out because palladium nanoparticles often have a vacancy in their center and vacancies within them. The methodology of electrically driving this system was discussed at ICCF-17 [22–24] and -18 [25–27]. Input power is defined as *V*I*. There is no thermoneutral correction in denominator.

Therefore, the observed incremental power gain is actually a lower limit. The instantaneous power gain (power amplification factor (non-dimensional)) is defined as $P_{\rm out}/P_{\rm in}$. As discussed above, the energy is calibrated by at least one electrical joule control (ohmic resistor) used frequently, and with time integration for additional energy validation. The output of the component is compared to the output of the precisely driven ohmic control.

The preloaded, stabilized components were driven by a DC voltage circuit up to 2000^+ V rail voltage. The duty cycle was split with about half going to a control portion consisting of a carefully controlled electrical DC pulse into an ohmic resistor which was used to thermally calibrate the calorimeter. We rely on three to five diagnostics to look for putative excess power gain in any sample, and time integration for putative excess power gain or excess energy gain. The presence of possible incremental power gain and possible energy gain are derived several ways to minimize the possibility of a false positive. Two of the methods use time integration for calculating total energy gain and thus command the most believability. Generally, at least three methods of verification are pooled to derive the sample activity. We use input-power-normalized delta-T (delta-$T/P_{\rm in}$), input power normalized heat flow (delta-HF/$P_{\rm in}$), and both single pole and double pole calorimetry, 5 and the new metric: ($\langle E_{\rm out}\rangle$ 5 min/$P_{\rm in}$), to determine the possible presence of excess energy gain.

Although small in size, this NANOR®-type preloaded LANR device is actually not *de minimus* because the LANR excess power density is more than 19,500 W/kg of nanostructured material [22–24] and the carbon footprint is zero. NANOR®-type CF/LANR quantum electronic components have enabled the way to higher instantaneous power gain, total energy gain, imaging [27], emissions [26,27], open demonstrations [23], and a better understanding of the impact of applied magnetic fields [25], electrical transconduction [16,22–27], and things that quench the desired reactions (as presented at ICCF 17–19).

Some of the results presented here were done at JET Energy and others were conducted at MIT using an

independent operation with a verified system to assess the possible presence of excess energy gain. At JET Energy, a custom controlled driving system, the NANOR Explorer™ is used linked to a high voltage or current source coupled to the NANOR-type LANR system. Compared to most systems, it provides an improved method of current control, enabling an improved and better paradigm system and the ability to evolve paradigms. At MIT, the runs were driven by a programmable Keithley current source, controlled by Python. The input powers were initially designed to be below 100 mW to increase the safety at the educational institution during the month-long runs and to facilitate a rapid time constant, although some NANOR®-type components have been driven up to the two watt level.

4. Two Driven States in the Same Run

4.1. Aqueous

Figure 1 shows the calorimetry (including incremental power gain) and the rate of "XSH"- and H_2-production of an aqueous Ni ordinary water system (Pt anode, PHUSOR®-type). Two modes in a single run for this electrically driven system is revealed. One mode makes much heat, and the other makes much evolved hydrogen gas.

4.2. Aqueous – anti-Stokes with XSH

Shown in Fig. 3 are two spectra of the same LANR aqueous component resolved by dual wavelength CMORE spectroscopy. The two modes (responses) are the undriven "off"-state, and the optimal operational state, the "Desired Active Mode", where "excess" energy is being released. Note how the "XSH" mode can be distinguished in its CMORE spectra observed by a unique reflected optical backscatter along with the reflected optical beams. Note the increase of the anti-Stokes peak from the active state of an aqueous Nickel/H_2O/Pt system.

Figure 3 reveals, and confirms the existence of, the two different electrically driven states beyond "off": "on-" (not active, no XSH), and "on+" (active, with XSH) for an aqueous CF/LANR system as revealed by calorimetry (and also by hydrogen evolution and by ohmic conductivity).

4.3. Nanomaterial

Several reports demonstrated that several electrical transconduction states exist, but that only one is active, desired, and capable of producing "XSH" [1,3–11]. To determine the effectiveness of the heat source, Fig. 4 is set of curves which presents the results of the same experiment, but which plots the temperature rise (delta-T in °C) of the preloaded NANOR®-type LANR component and the ohmic control with both normalized to input electrical power. This derived value, delta-T/P_{in}, is important because it enables semiquantitative determination of the incremental power gain. Figure 4 reveals the two different electrically driven states beyond "off" : "on-" (not active, no XSH), and "on+" (active, with XSH) for a nanomaterial CF/LANR system as revealed by calorimetry (and ohmic conductivity).

The top of Fig. 4 shows the differential temperature rise normalized to input electrical power for the preloaded NANOR®-type LANR component, and for the case with no input power and for the case of input to the ohmic thermal control, located at the core. These curves show the dT/Pin ratios, which enable determination of the power gain, both in the XSH region and after the avalanche behavior, for a ZrO_2–NiD NANOR®-type component. The region of the avalanche is labeled. The x-axis represents time, and each count represents 6 s. The y-axis on the left-hand side represents electrical input power in watts. Each of the outputs is read off of the right-hand side. The y-axis on the right-hand side represents the amount of temperature rise (differential temperature increase) normalized (i.e., divided by) to the electrical input power. The units of this axis are in °C/W. A calibration pulse, used for accuracy and precision check of voltage and current measurement, are again also shown at the beginning and end (not labeled) of the run.

Because these curves plot the temperature rise normalized to input electrical power as a function of time, the ratios can be used to estimate incremental power gain. That is done here by taking the ratio of the response of the

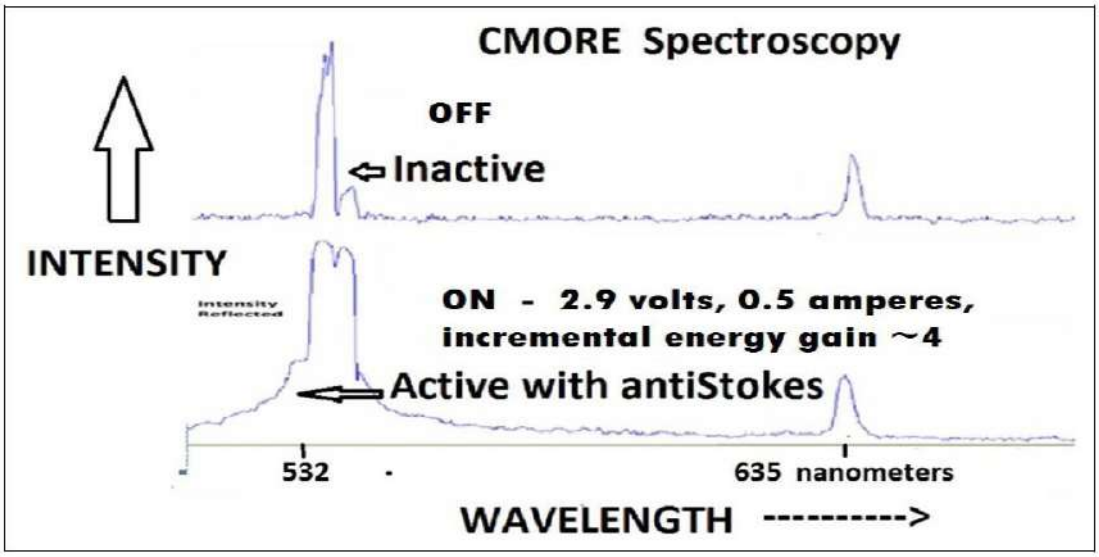

Figure 3. Two electric-driven modes revealed by CMORE spectroscopy. This figure shows CMORE spectra. The system used was an aqueous Ni ordinary water system (Pt anode). These are two CMORE spectra of a CF/LANR Aqueous Nickel/H_2O/Pt system in two electrical states; "off" top, and active XSH mode (*bottom*). Shown are the reflected optical intensities as a function of wavelength (increasing to the right side).

NANOR (green) to the ohmic control (orange). Compare the delta-T output normalized to input power for preloaded NANOR®-type LANR component to the thermal (ohmic) control, delta-T/P_{in}. By comparing that ratio, note the active preloaded LANR quantum electronic component again clearly shows significant improvement in thermal output, here input-power-normalized compared to a standard ohmic control (a carbon composition resistor). Observe that despite lower input electrical power to the NANOR®, the temperature rise normalized to input electrical power observed in the core was higher than expected, as compared to the ohmic control.

The graph therefore shows quite clearly a demonstrated active over-unity thermal output power from the NANOR®-type cold fusion (LANR) component, before the electrical avalanche.

The lower graph presents the power gain of the ZrO_2–NiD NANOR®-type component CF/LANR component as a function of time, and shows that the XSH which is generated decreases with high input power, eventually reverting to normal, ordinary, resistor-like operation after the electrical avalanche.

Note the optimal power gain of NANOR®-type cold fusion components is found far below the breakdown voltage and that the power gain decreases continuously as the electrical avalanche threshold is approached. Beyond the region of electrical avalanche, the previously active preloaded LANR quantum electronic components then give a thermal output similar to a standard ohmic control (a carbon composition resistor).

Despite driving at higher input electrical power, on other side of the electrical avalanche, these NANOR®-type components act as little more than electrical resistors which are conventional, not over-unity, and therefore are functionally "dead" with respect to producing XSH. Although this appears limiting in some ways, this phenomena does provide yet an additional control to check calorimetry beyond the measurements involving simply using a simple ohmic, thermal control. Therefore, driving a component into this region thus adds an additional verification of the actual XSH which is developed in these studies.

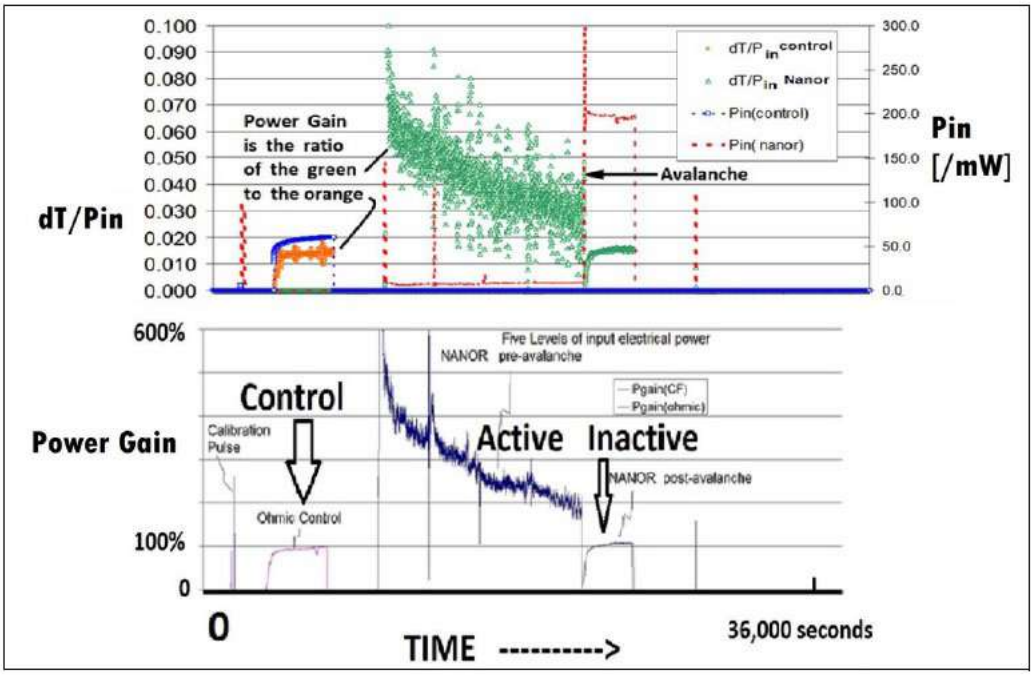

Figure 4. Two electric-drive modes revealed for a nanomaterial LANR systems nanomaterial LANR system by calorimetry. (*top*) This figure shows calorimetry (including incremental power gain, and the rate of XSH- and H_2– production). The system used was a dry preloaded ZrO_2–NiPdD NANOR®-type component (NANOR 7-7; ZrO_2NiD; results shown at ICCF-19 [16,22–24]. The delta-$T/P_{\rm in}$ ratios enable general estimates of the output power. The region of the avalanche is labeled. The x-axis represents time. The $y-$axis on the right-hand side represents electrical input power in watts. The y-axis on the left-hand side represents the amount of temperature rise (differential temperature increase) normalized (i.e., divided by) to the electrical input power. The units of this axis are in s°C/W. (*bottom*) This graph presents the power gain of the ZrO_2–NiD NANOR®-type component CF/LANR component as a function of time, and shows that the XSH which is generated decreases with high input power, eventually reverting to normal, ordinary, resistor-like operation after the electrical avalanche.

4.4. Nanomaterial – anti-Stokes with XSH

Figure 5 shows the two different electrically driven states beyond "off": "on−" (not active, no XSH), and "on+" (active, with XSH) for a nanomaterial CF/LANR system as revealed by CMORE spectroscopy, revealing the active, desired CF/LANR state by anti-Stokes emissions. Shown are the overlaid spectra of the three different electronic modes ("states"), each resolved by dual wavelength coherent electric-driven volume-enhanced reflection spectroscopy for the same preloaded ZrO_2PdD NANOR®-type CF/LANR component in three different electrical drive modes. The graph presents the output as intensity as a function of wavelength, as returned by backscatter along with the reflected optical beams from the volume-enhanced interactions. Labelled are the assignments of the anti-Stokes peaks to Zirconia and PdD.

In Fig. 5, intensity is shown as a function of wavelength, as returned by backscatter along with the reflected optical beams. One state is the unwanted electrical avalanche mode [16,22]. Another state is the desired optimal operational state (the active excess XSH mode), where excess energy is being released. The third state is the state where the electrical drive is "off". For the desired active XSH-producing state, the nanomaterial NANOR®-type CF/LANR component was properly, correctly electrically driven at 2500 V which produced an electrical current of

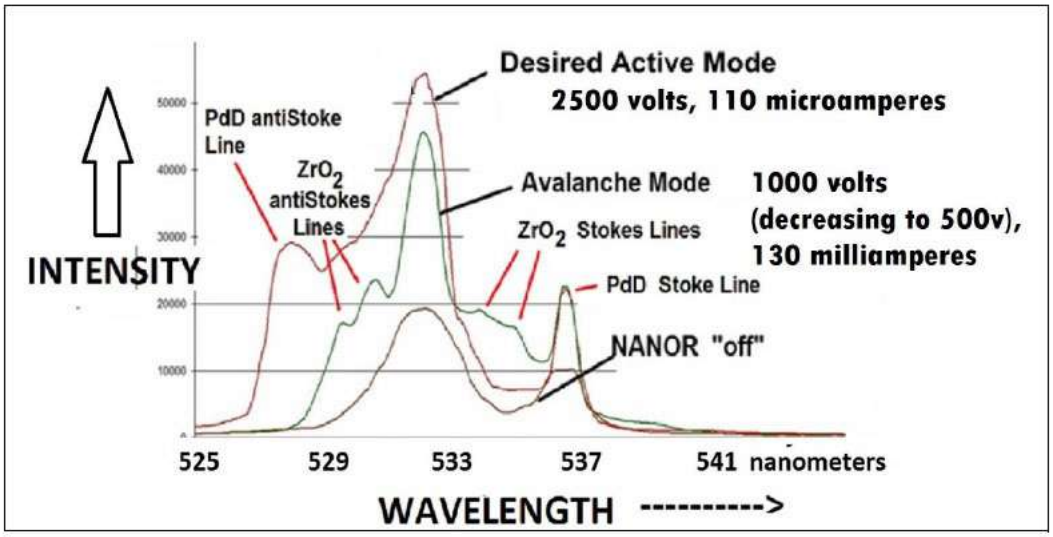

Figure 5. CMORE spectra of ZrO_2PdD NANOR®-type CF/LANR. These are the overlaid spectra of the three different electronic states optical signatures for the same preloaded ZrO_2PdD NANOR®-type CF/LANR component in three different electrical drive modes. Shown are spectra of the same NANOR®-type CF/LANR component (Nanor® 7-6) in three different electronic states, resolved by dual wavelength coherent electric-driven volume-enhanced reflection spectroscopy. Labeled are the assignments of the anti-Stokes peaks to zirconia and PdD.

about 0.11 mA. The sample maintained its high impedance (compared to that seen during avalanche mode) during the very short run, and there was no electrical avalanche quenching the desired reactions.

Note that the avalanche anti-Stokes peaks are many, and they are lower energy than the XSH mode-produced anti-Stokes peak (described below). By contrast, successful cold fusion is heralded by a large increase in the anti-Stokes to Stokes (aS/S) ratio, and the generated anti-Stokes peak for the desired and XSH-producing state is very different from the avalanche-generated many anti-Stokes peaks. That XSH-related peak is singular and at higher energy. This distinguishing, higher energy, single, anti-Stokes peak (which also heralds phonon gain) is also not seen in the off state or the avalanche (undesirable) mode. Analysis of the phonon gain heralds $\sim 7^{\pm 0.15}$ acoustic phonons assisting nuclear reactions and a core peak calculated Stokes temperature of circa 1645 K. Therefore, these findings confirm a role for PdD acoustic phonons, in the loaded lattice, during successful CF/LANR which produces XSH.

4.5. Independent confirmation

Run EF9-160410A of NANOR 8-2: ZrO_2PdD At MIT, Run EF9-160410A was the sixth run of a Series 8-2 Nanor-type LANR component. Two-pole calorimetry examined the input and output power and energy as a function of time for run EF9-160410A for an ohmic control and NANOR 8-2. Figure 6 shows the "XSH"-phase space is here represented in qualitative approximation by delta-$T/P_{\rm in}$, separates out into at least three distinct groups. They are the states represented by the ohmic control, and by the NANOR-type component exhibiting pre-avalanche or post-avalanche behavior.

Figure 6 (*top*) shows the electrical impedance (resistance) of the ohmic control and then NANOR-type component at several input power levels as a function of time. The ohmic control is a nominal 1 MΩ resistor. Note that the resistor performs as approximately a more straight horizontal line. It is essentially a "constant".

Notice also that there is some avalanche breakdown in the second region of NANOR drive. There is, in fact,

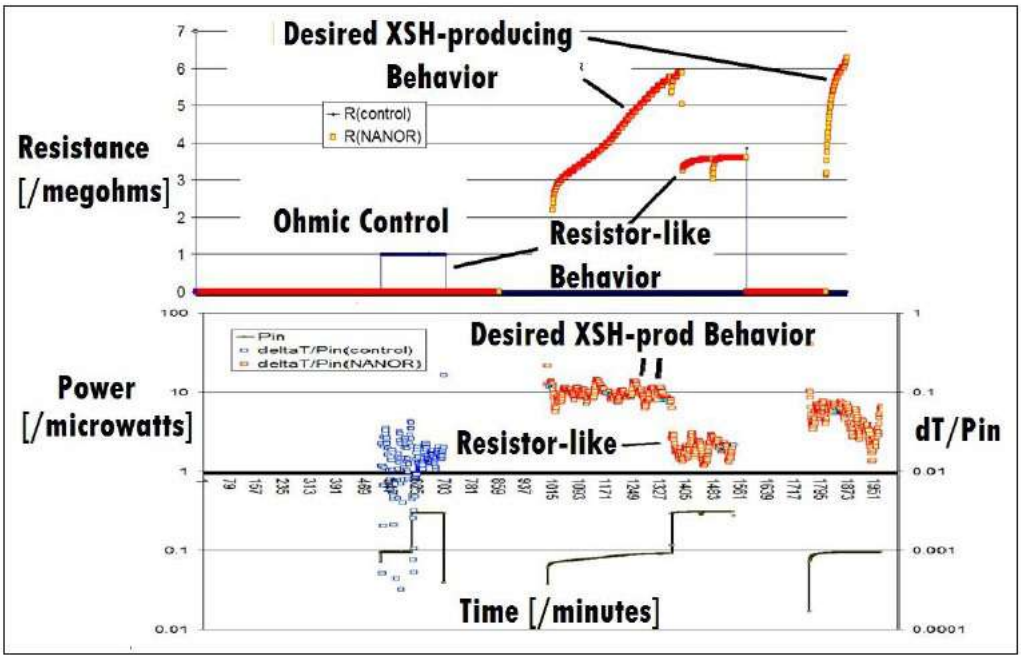

Figure 6. (*top*) The two terminal electrical impedance during run EF9-160410A for NANOR 8-2 as a function of time.(*bottom*) - $\mathrm{d}T(*)/P_{\mathrm{in}}$ of run EF9-160410A for NANOR 8-2 as a function of time. The star indicates that for the calorimetry, a single linear shift was used to balance $\mathrm{d}T$.

synchronous loss of XSH only before the electrical avalanche, as will be seen below. After the electrical avalanche, there is a conversion to ohmic resistance behavior. These regions are clearly labeled in the figure.

Figure 6 (*bottom*) shows the result, and is the input-power-normalized incremental temperature gain $(\mathrm{d}T(*)/P_{\mathrm{in}})$ as a function of time for both the ohmic control and the NANOR-type component 8-2 in run EF9-160410A. There is good input power overlap and therefore Fig. 6 heralds a strong demonstration of excess power gain, and also calibrates by showing exactly what happens with electrical breakdown, and that is normal ohmic behavior.

Notice there are again two states characterizing the NANOR-type component separate out. The upper is the higher impedance XSH producing mode, and the lower is the more conductive non-XSH mode. They separate out with an incremental power gain matching the other methods of measurement.

Other NANOR type had higher incremental gains pre-avalanche, up to an estimated $100\times$ input, decreasing to $8\times$ input very close to the avalanche. Several also had confirmation by input power normalized heat flow. The two states are clearly shown in Table 1. Table 1 shows the incremental power gains pre-avalanche and post-avalanche. The incremental power gain pre-avalanche was $\sim$500% over the input power. In this run, there was a very small excess energy of 13,000 μJ. These power gains for these components were evanescent, and that value decreased over the next two weeks to half that XSH by run EF9-160421A.

Table 1. Qualitative incremental power gains for NANOR 8-2.

Excess power gains for run EF9-160410A		
Method	Pre-avalanche (%)	Post-avalanche
dT/P_{in}	500	100% (normal)
$\Delta[\langle E_{out}\rangle - \langle E_{in}\rangle]/P_{in}$	250–350	100% (normal)

5. Interpretation

5.1. Origin of two different states in aqueous LANR systems

The quasi-one-dimensional (Q1D) model for hydrogen loading of an electrode describes the loading flux of hydrogen by the ratio of two energies (electric order to thermal disorder ratio). From the metallurgical point of view (POV), from the metal surface, atomic deuterons either enter the metal ("are loaded"), remain on the surface, or form diatomic deuterium gas bubbles (D_2). The gas bubbles (D_2) are undesirable producing low dielectric constant layers in front of the electrode, obstructing the electrical circuit. And so, at the metal surface, four components of deuteron flux must be considered [12–14], fundamental to the entire understanding of these phenomena. These deuteron fluxes include entry into the metal (J_E), movement to gas evolution (J_G), and an extremely tiny loss by potential fusion reactions (J_F). There is conservation of deuterons with the exception of a loss (J_F) to all putative fusion reactions, which are extremely small, even when present.

From the mathematical POV, the three components of flux are the entry of deuterons to the lattice (J_E), gas evolution (J_G), and the desired fusion reactions (J_F).

$$J_D = B_D * \frac{d[D(z,t)]}{dz} - \mu_D * [D(z,t)] * \frac{d\Phi}{dz}. \tag{1}$$

The deuteron flux, J_D, depends on deuteron diffusivity (B_D) and electrophoretic mobility (μ_D), and the applied electric field intensity. At any molecular site across the heavy water solution, the applied electrical energy is a tiny fraction compared to $k_B T$, so the deuterons migrate by drift ellipsoids of L- and D-deuteron defects in the applied electric field creating a ferroelectric inscription [28,29]. This D-defect conduction/polarization process augments other charge carriers, ionic drift, space charge polarization, and clathrates. The resultant D-defect migration produces a cathodic fall of deuterons and an E-field contraction so that most of the voltage drop is at the interface in front of the electrode surface. This concentration polarization may produce very large local electric field intensities, possibly ranging from 10^4 to 10^7 V/cm.

Dividing each flux by the local deuteron concentration yields the first order deuteron flux constants, k_E, k_G, and k_F (cm/s), respectively, which are the basis of the rest of the discussion, and Eq.(2).

$$k_e = (\mu_D * E) - (k_g + k_f). \tag{2}$$

Equation (2) is the deuteron loading rate equation. It relates cathodic deuteron gain from the applied electric field to the loss of deuterons from gas evolution and fusion, and teaches many things. The deuteron loading rate equation shows that the deuteron gain of the lattice (through the first order loading flux rate (k_E)) is dependent upon the applied electric field MINUS the flux rate losses of deuterons from gas evolution (k_G) and fusion (k_F). The deuteron loading rate equation, Eq. (2), reveals that desired LANR reactions are quenched by electrolysis, which is opposite conventional "wisdom" that LANR is 'fusion by electrolysis'.

Equation (2) also heralds that LANR can be missed by insufficient loading, contamination (effecting k_E, by protons or salt), and by the evolution of D_2 gas, which all inhibit the desired LANR reactions [12–14,7–11], and leading to the OOP manifolds.

The modified deuteron flux equation (Eq. (3)) is Eq. (2) changed by substituting the Einstein relation.

$$k_{\mathrm{e}} = \frac{B_{\mathrm{D}} * qV}{L * (k_{\mathrm{B}} * T)} - (k_{\mathrm{g}} + k_{\mathrm{f}}). \tag{3}$$

The first term now has geometric, material factors, and the ratio of two energies (the applied electric energy organizing the deuterons divided by $k_{\mathrm{B}} * T$, thermal disorder).

The modified deuteron flux equation reveals how competitive gas evolving reactions and the applied electric field energy to thermal energy ($k_{\mathrm{B}} * T$) are both decisive in controlling the deuteron loading flux in palladium.

Successful LANR experiments are dominated by this ratio reflecting the "war" between applied electrical energy which is organizing the deuterons versus their randomization by thermal disorganization. The two terms are the first order deuteron loss rates by gas evolution and the desired fusion process(es). The Phusor®-type LANR device is a metamaterial and its physical structure enhances the metallurgic properties of loaded palladium [30]. This metamaterial change alters the electric field distribution in the high impedance solution, producing continuous deuteron flux within the loaded palladium. This is unique to this device creating a distinguishing electric field (E-field) distribution different from customary wire-wire, and other systems. This is significant and with marked more XSH.

5.2. Origin of two states in nanomaterials

Previously, we reported that the optimal power gain of NANOR®-type cold fusion components is only found below the breakdown voltage, and that the power gain decreases continuously as the electrical avalanche threshold is approached. Once the electrical avalanche has occurred, there is complete loss of the desired XSH [15,22–24]. Avalanche behavior with three regions were first observed by Swartz with ZrO–NiH NANOR®-type component. Since then, cold fusion nanomaterials, in general, and NANOR®-type LANR components (derived from them), in particular, have been repeatedly found to have distinct regions of performance on each side of the electrical avalanche. Beyond the region of electrical avalanche, the previously active preloaded LANR quantum electronic components then give a thermal output similar to a standard ohmic control (a carbon composition resistor). Therefore, this transformation of active CF/LANR components from active to inactive states has been critical to successfully controlling CF/LANR, and is critical to understanding how to engineer these systems.

For a materials POV, the nanostructured material is a composite distribution of nanostructured ferromagnetic "islands" separated among a vast dielectric zirconia "ocean". The dielectric zirconia embeds uncountable numbers of nanostructured metal ternary alloy islands. The high resistance occurs because the zirconia dielectric matrix is insulating at low voltage and it keeps the nanoscale metal islands electrically separated and prevents the aggregation of the islands. Each nanostructured island acts as a short circuit elements during electrical discharge. One hypothesis of the XSH is that these "islands" allow deuterons to form a hyperdense state in each island, where the deuterons thereafter are able to be sufficiently close together to fuse and form ^{4}He*, by some pathway not known involving paired deuterons or possibly more.

6. Conclusion

6.1. Solid evidence of two states

There is now sterling evidence of the existence of two states in electrically driven CF/LANR systems (Table 1). Two different methods (calorimetry and CMORE spectroscopy) confirm each other for both aqueous and dry preloaded LANR systems, and corroborate the existence of two electrically driven states – one inactive and the other active (XSH-producing).

As a corollary, both aqueous and nanostructured LANR systems, when active, have distinct calorimetric and CMORE anti-Stokes-XSH linked signatures. Thus, knowledge and use of these two signatures has considerable value when seeking active systems, controlling those systems, and understanding some past difficulties.

6.2. Implications of two states in CF/LANR

What is the implication of recognizing which, of two (or more) electrically driven states, is active? First, this may explain why some CF/LANR systems fail to create "XSH".

Second, it must be added to the other pitfalls involving metallurgy, electrochemistry, isotopic loading, contamination and quenching, and failure to drive at the OOP. In CF/LANR, understanding the existence of two states, and OOP Technology, opens the door to more reproducible systems. This reveals that the other reactions, most of which are unwanted and quench the desired reactions and pathways.

Third, Why is the recognition of two electrically driven states in CF/LANR very important? The most important reasons is because ONLY the more difficult-to-obtain pathway leads to the desired, sought XSH.

Table 2. Evidence of two driven states (modes)

√	Calorimetry showing XSH when active only
√	Phase change c/w XSH
√	Change in electrical conductivity c/w XSH
√	Change in anti-Stokes spectrum c/w XSH
√	OOP behavior c/w two states (suggestive)
	Aqueous CF/LANR systems
√	OOPs - indirect evidence c/w two states (ICCF-7,9,10,14)
√	Direct proof of two states (ICCF-21)
	Dry Nanostructured CF/LANR systems
√	OOPs - indirect evidence c/w two states(ICCF-17–20)
√	Direct proof of two states (ICCF-19,20)
√	Confirmed proof of two states (ICCF-21)

Acknowledgments

The author acknowledges and thanks, for their very helpful comments, editorial assistance, and support, Gayle Verner, Peter Hagelstein, Alex Frank, Florian Metzler, Brian Ahern, and Jeff Driscoll, for their help, ideas and suggestions. This effort was supported by JET Energy Inc. and the New Energy Foundation. NANOR® is a registered trademark of JET Energy, Incorporated. NANOR®-technology and other technology described here are protected by patents pending.

References

[1] M.R. Swartz, Survey of the Observed Excess Energy and Emissions In Lattice Assisted Nuclear Reactions, *J. Scientific Exploration* **23** (4) (2009) 419–436.

[2] M.H. Miles, R.A. Hollins, B.F.Bush, J.J. Lagowski and R.E. Miles, Correlation of excess power and helium production during D_2O and H_2O electrolysis using palladium cathodes, *J. Electroanal. Chem.* **346** (1993) 99–117.

[3] M.R. Swartz, Excess power gain using high impedance and codepositional LANR devices monitored by calorimetry, heat flow, and paired stirling engines, *Proc. ICCF14* **1** (2008) 123, ISBN: 978-0-578-06694-3, 123, (2010); www.iscmns.org/iccf14/ProcICCF14a.pdf.

[4] M.R. Swartz, G. Verner et al., Non-thermal near-IR emission from high impedance and codeposition LANR devices, D.J. Nagel and M.E. Melich (Eds.), *Proc. ICCF14* **1** (2008) 343, ISBN: 978-0-578-06694-3, 343, (2010); www.iscmns.org/iccf14/ProcICCF14a.pdf

[5] M.R. Swartz, Photoinduced excess heat from laser-irradiated electrically-polarized palladium cathodes in D_2O, *Condensed Matter Nuclear Science*,Peter L. Hagelstein and Scott Chubb (Eds.), *Proc. ICCF-10*, NJ, ISBN 981-256-564-6, 213-226 (2006).

[6] M.R. Swartz and G. Verner, Excess heat from low electrical conductivity heavy water spiral-wound Pd/D_2O/Pt and Pd/D_2O-PdCl2/Pt devices, *Condensed Matter Nuclear Science, Proc.ICCF-10*, World Scientific, NJ, ISBN 981-256-564-6, 29-44; 45-54 (2006).

[7] M.R. Swartz, Consistency of the biphasic nature of excess enthalpy in solid state anomalous phenomena with the quasi-1-dimensional model of isotope loading into a material, *Fusion Technol.* **31** (1997) 63–74.

[8] M.R. Swartz, Optimal operating point manifolds in active, loaded palladium linked to three distinct physical regions, D.J. Nagel and M.E. Melich (Eds.), *Proc. ICCF14* **2** (2008) 639, ISBN: 978-0-578-06694-3, 639 (2010); www.iscmns.org/iccf14/ProcICCF14b.pdf.

[9] M.R. Swartz, Optimal operating point characteristics of nickel light water experiments, *Proc. ICCF-7*, 1998.

[10] M.R. Swartz, improved electrolytic reactor performance using p-notch system operation and gold anodes, *Transactions of the American Nuclear Association*, Nashville, TN. Meeting, (ISSN:0003-018X publisher LaGrange, Ill) **78** (1998) 84–85.

[11] M.R. Swartz, Can a Pd/D_2O/Pt device be made portable to demonstrate the optimal operating point?, *Condensed Matter Nuclear Science*, Peter L. Hagelstein and Scott Chubb (Eds.), *Proc. ICCF-10*, World Scientific, NJ, ISBN 981-256-564-6, 29-44; 45-54 (2006).

[12] M.R. Swartz, Quasi-one-dimensional model of electrochemical loading of isotopic fuel into a metal, *Fusion Technol.* **22** (2) (1992) 296–300 .

[13] M.R. Swartz, Isotopic fuel loading coupled to reactions at an electrode, *Proc. ICCF4* **2** (1993) 429; *Fusion Technol.* **26** (4T) (1994) 74–77, www.lenr-canr.org/acrobat/EPRIproceedinga.pdf.

[14] M.R. Swartz, Codeposition of palladium and deuterium, *Fusion Technol.* **32** (1997) 126–130.

[15] M.R. Swartz, Investigations of heat after death , in press.

[16] M.R. Swartz, P. Hagelstein and G. Verner, Impact of electrical avalanche through a ZrO_2–NiD nanostructured CF/LANR component on its incremental excess power gain, *ICCF-19*, *J. Condensed Matter Nucl. Sci.* **19** (2016) 287.

[17] M.R. Swartz, Optical detection of phonon gain distinguishes an active cold fusion/LANR component, *J. Condensed Matter Nucl. Sci.* **20** (2016) 29–53, www.iscmns.org/CMNS/JCMNS-Vol20.pdf.

[18] M.R. Swartz and Peter L. Hagelstein, Increased PdD anti-Stokes peaks are correlated with excess heat mode, *J. Condensed Matter Nucl. Sci.* **24** (2017) 130–145.

[19] M.R. Swartz, Increase of an anti-Stokes peak at the cathode of an electrically driven, active aqueous nickel/H_2O/Pt system, *J. Condensed Matter Nucl. Sci*. **27** (2018) 1–8.

[20] C.V. Raman, *Scientific Papers of Sir C.V. Raman*, *The Scattering of Light*, Vol. 1, S. Ramaseshan (Ed.), India Indian Academy of Sciences, Bangalore, 1988.

[21] M.R. Swartz, Charles Haldemann, Alan Weinberg and Brian Ahern, possible deuterium loss during excess heat from ordinary water-carbonate electrolyte using nickel, **29** *J. Condensed Matter Nucl. Sci.* (2018).

[22] M.R. Swartz and P.L. Hagelstein, Energy Gain From Preloaded ZrO_2–PdNi–D Nanostructured CF/LANR Quantum Electronic Components, *J. Condensed Matter Nucl. Sci.* **13** (2014) 528, www.iscmns.org/CMNS/JCMNS-Vol13.pdf.

[23] M.R. Swartz and P.I. Hagelstein, Demonstration of energy gain from a preloaded ZrO_2–PdD nanostructured LENR quantum electronic device at MIT, *J. Condensed Matter Nucl. Sci.* **13** (2014) 516, www.iscmns.org/CMNS/JCMNS-Vol13.pdf.

[24] M.R. Swartz, G. Verner, J. Tolleson and P. Hagelstein, Dry, preloaded NANOR®-type CF/LANR components, *Current Sci.* **108** (4) (2015) 595.

[25] M.R. Swartz, G. Verner, J. Tolleson, L. Wright, R. Goldbaum, P. Mosier-Boss and P. Hagelstein, Amplification and restoration of energy gain using fractionated magnetic fields on ZrO_2–PdD nanostructured components, *J. Condensed Matter Nucl.*

Sci. **15** (2015) 66, www.iscmns.org/CMNS/JCMNS-Vol15.pdf.

[26] M.R. Swartz, Incremental high energy emission from a ZrO_2–PdD nanostructured quantum electronic component CF/LANR, *J. Condensed Matter Nucl. Sci.* **15** (2015) 92.

[27] M.R. Swartz, . Verner, J. Tolleson, L. Wright, R. Goldbaum and P. Hagelstein,, Imaging of an ative NANOR®-type LANR component using CR-39, *J. Condensed Matter Nucl. Sci.* **15** (2015) 81.

[28] M.R. Swartz, Dances with protons – ferroelectric inscriptions in water/ice relevant to cold fusion and some energy systems, *Infinite Energy* **44** (2002) 64–70.

[29] M.R. Swartz, Water is best, *Infinite Energy* **134** (2017) 16–29.

[30] M.R. Swartz and G. Verner, The Phusor®-type LANR cathode is a metamaterial creating deuteron flux for excess power gain, D.J. Nagel and M.E. Melich (Eds.), *Proc. ICCF14 Proc. ICCF14* **2** (2008) 458, ISBN: 978-0-578-06694-3, 458, (2010); www.iscmns.org/iccf14/ProcICCF14b.pdf.